



CHORUS

This is the accepted manuscript made available via CHORUS. The article has been published as:

Polaron-induced metal-to-insulator transition in vanadium oxides from density functional theory calculations

Jasleen Kaur, Manas Likhith Holekevi Chandrappa, Chi Chen, and Shyue Ping Ong

Phys. Rev. B **107**, 125162 — Published 30 March 2023

DOI: [10.1103/PhysRevB.107.125162](https://doi.org/10.1103/PhysRevB.107.125162)

Polaron-induced Metal-to-Insulator transition in Vanadium Oxides from Density Functional Theory Calculations

Jasleen Kaur

*Department of Materials Science and Engineering,
University of California San Diego, 9500 Gilman Dr,
Mail Code 0448, La Jolla, CA 92093-0448, United States*

Manas Likhith Holekevi Chandrappa, Chi Chen, and Shyue Ping Ong*

*Department of NanoEngineering, University of California San Diego,
9500 Gilman Dr, Mail Code 0448, La Jolla, CA 92093-0448, United States*

Abstract

Vanadium oxides have been extensively studied as phase-change memory units in artificial synapses for neuromorphic computing due to their metal-insulator transitions (MIT) at or near room temperature. Recently, injection of charge carriers into vanadium oxides, e.g., via optically via a heterostructure, has been proposed as an alternative switching mechanism and also potentially as a means to tune the MIT temperature. In this study, we explore the formation of small polarons in the low temperature (LT) insulating phases for V_3O_5 , VO_2 and V_2O_3 and the barriers to their migration using density functional theory calculations. We find that V_3O_5 exhibits very low hole and electron polaron migration barriers (< 100 meV) compared to V_2O_3 and VO_2 , leading to much higher estimated polaronic conductivity. We also link the relative migration barriers to the amount of distortion that has to travel when the polaron migrate from one site to another. Polarons in V_3O_5 also have smaller binding energies to vanadium and oxygen vacancy defects. These results suggest that the triggering of the MIT via injection of charge carriers are due to the formation of small polarons that can migrate rapidly through the crystal.

I. INTRODUCTION

Vanadium oxides[1, 2] have a wide range of applications in optoelectronic devices, gate dielectrics, and thin-film transistors[3, 4]. In particular, they have attracted much attention as phase-change memory (PCM) units for neuromorphic computing [5–7] due to their metal-insulator transitions (MIT) at near room temperature. Neuromorphic computing, which is modelled on the mammalian brain, is a highly promising alternative to traditional von Neumann architectures with potentially have superior efficiency and lower power consumption. [5, 8–12]. One approach to implement the artificial synapse in neuromorphic computing is via nonvolatile resistive switching, which can be achieved via the MIT in PCMs with high scalability and fast operation speed [5, 7].

Among vanadium oxides (Figure 1), VO_2 and V_2O_3 , with MIT temperatures (T_c) of 340 K[14] and 160 K[6], respectively, have received the majority of interest from researchers[10, 15–20]. Many studies have been done to understand different ways in which MIT can be triggered in these two materials, including point defect formation[6, 14], strain introduction [10],

* onbsp@eng.ucsd.edu

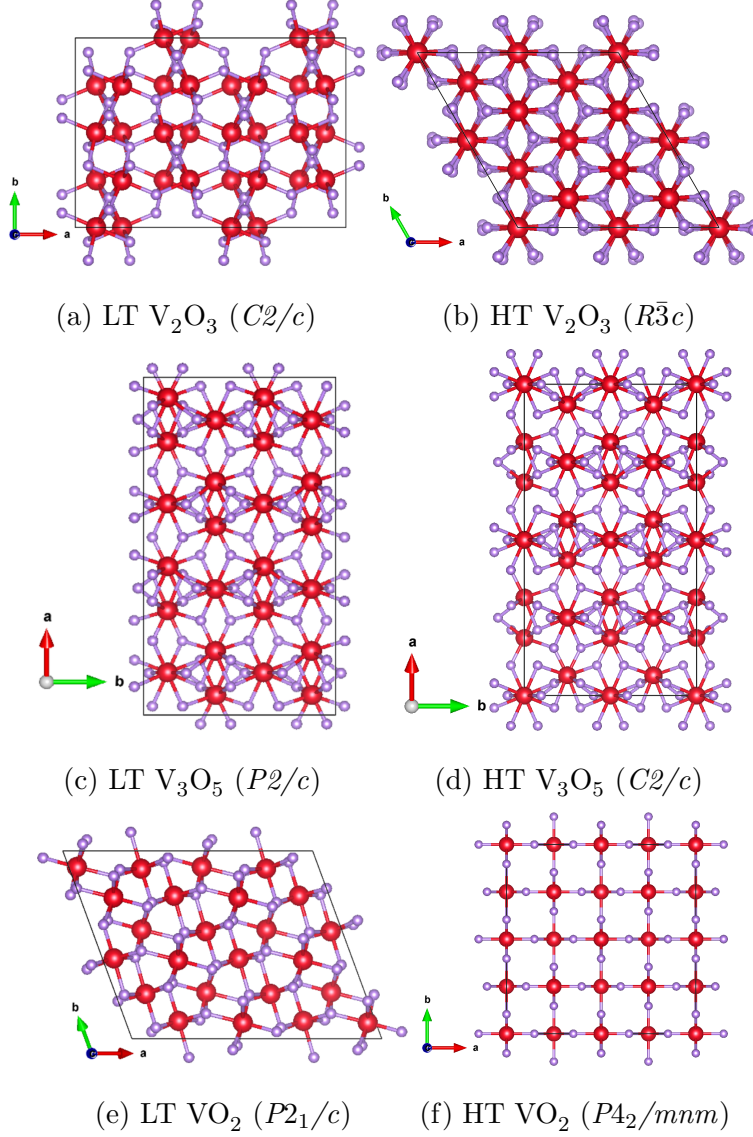


FIG. 1: VESTA representation of different low-temperature (LT) and high-temperature (HT) V-O structures (with space groups) obtained from Materials Project[13]. Vanadium and oxygen atoms are represented by red and lavender spheres, respectively.

and optically[15] or electrically[19] driven processes. Less attention has been given to V_3O_5 due to its relatively high T_c of 428 K[21], despite several potential advantages. For instance, unlike VO_2 , a device incorporating V_3O_5 can operate at much higher junction temperatures without requiring active cooling to avoid undesired thermally-induced switching[22]. In addition, due to its small volume and symmetry change at the phase transition[23], the device can undergo repeated cycling without experiencing significant damage from mechanical stress[24]. However, to exploit these advantages, it is necessary to explore alternative

PCM triggering mechanisms. For instance, one approach demonstrated in a previous work is to utilize a CdS/ V_3O_5 heterostructure[21] wherein photo-induction results in direct transfer of electrons from CdS into V_3O_5 to induce nonvolatile resistive switching at room temperature. In this previous work, the switching was attributed to a reduction in the band gap as a result of the formation of negatively-charged oxygen vacancies.

The introduction of electrons (or holes) in a dielectric crystal may result in localization of charge and an accompanying local lattice distortion, a quasi-particle known as a polaron. Polaron-induced MIT has been observed in several oxides of vanadium, nickel, titanium, europium, manganese.[25–29]. Polarons have also been observed experimentally in V_3O_5 by Kumar *et al.*[30] However, to the authors’ knowledge, there have been no computational studies of polaron formation and migration in the different oxides of vanadium. Such insights are key to the understanding the mechanism of polaron-induced MIT.

In this work, we perform a comprehensive study of polaron formation and migration in three vanadium oxides - V_2O_3 , VO_2 and V_3O_5 - using density functional theory (DFT) calculations. A greater focus is placed on the less well-studied V_3O_5 . We demonstrate that both hole and electron polaron formation is favorable in V_3O_5 , and these polarons have much lower migration barriers in comparison to polarons in VO_2 and V_2O_3 . We also find that polarons are less strongly bound to vacancy defects in V_3O_5 compared to VO_2 and V_2O_3 . These findings suggest that V_3O_5 is much more tunable for polaron-induced MIT than VO_2 and V_2O_3 for neuromorphic computing.

II. METHODS

All DFT[31, 32] calculations were performed using Vienna *Ab initio* Simulation Package (VASP)[32–34] within the projector augmented wave(PAW) [35] approach. The Perdew-Burke-Ernzerhof (PBE) [36] Generalized Gradient Approximation (GGA) [37] functional was used with a plane wave cutoff of 520 eV. The energy and force convergence criteria were set to 10^{-4} eV and -0.02 eV/Å, respectively. The tetrahedron method with Blöchl corrections [38] was used for the insulating low-temperature (LT) phase. A Γ -centered k-point meshes of $1 \times 2 \times 2$ and $3 \times 4 \times 4$ was used for the structure relaxation and density of states (DOS) calculations, respectively, on $2 \times 2 \times 2$ supercells (containing 160, 256 and 144 atoms for V_2O_3 , V_3O_5 , and VO_2 , respectively).

All input generation and output analysis were performed using the Python Materials Genomics (pymatgen) library[39]. The LT structures were obtained from Materials Project (MP)[13]. To treat the localized V $3d$ electrons, Hubbard U parameters[40] of 2.78 eV [6], 3.5 eV [21] and 4.25 eV [14] were applied for V_2O_3 , V_3O_5 and VO_2 respectively, to reproduce the respective experimental band gaps[4].

A. Polaron localization

To introduce a polaron into V_xO_y (wherein x and y represents the V and O stoichiometry, respectively), an initial distortion was first applied in the fully-relaxed neutral supercell by changing the V-O bond lengths around each symmetrically distinct V site.[41, 42] Assuming hole and electron polarons to localize on V^{3+} and V^{4+} sites, respectively, a full structural relaxation was then performed with an electron added (electron polaron) or removed (hole polaron), with overall charge neutrality preserved via a compensating background charge.

Polaron localization was confirmed via Bader charge analysis[43] as well as charge density difference plot between the polaron containing and neutral supercell. The polaron formation energy was calculated using the following equation[44]:

$$E_p = E^{polaron}(N) - E^{undistorted}(N) \quad (1)$$

where $E^{undistorted}(N)$ is the total energy of the undistorted supercell with N electrons, and $E^{polaron}(N)$ is the total energy of supercell containing the polaronic distortion. A negative E_p indicates a stable (self-trapped) polaron localization.

B. Polaron migration barriers

For a polaron to migrate, the accompanying lattice distortion has to travel from one site to a neighboring site. An initial pathway is first constructed by linearly interpolating [41] all atomic coordinates between the initial (q_i) and final (q_f) ion positions. The atomic coordinates of an intermediate image q_x is therefore given by: $q_x = (1 - x)q_i + xq_f$, where $0 \leq x \leq 1$. A total of 7 images is used for interpolation. The static DFT energies of the linearly-interpolated images were first computed to provide an initial estimate of the polaron migration barrier. Thereafter, climbing image nudged elastic band (CI-NEB)[45] calculations were carried out to obtain the minimum energy pathway.

The polaronic electronic conductivity (σ) at 300K is then estimated using the following expression:[46]

$$\sigma = ne\mu_h = ne\frac{ega^2\nu_0}{k_B T} \exp\left(\frac{-\Delta E_b}{k_B T}\right) \quad (2)$$

where n is the polaron concentration, e is the electron charge, g is the geometric pre-factor, a is the jump distance, ν_0 is the characteristic phonon frequency, k_B is the Boltzmann constant, and T is the temperature. It has been found that $ega^2\nu_0/k_B T \approx 1$ cm²/Vs at 300 K for a variety of materials[46]. Therefore, by substituting this fraction to ≈ 1 , we can calculate the conductivity at 300 K, which depends on the migration barrier (ΔE_b).

C. Polaron binding energies

Vanadium[6] (v_V) and oxygen (v_O) vacancy[22, 47] defects are commonly found in vanadium oxides. Polarons can bind strongly to such defects.[48] To compute the binding energy of polarons to such defects, a vacancy defect is first introduced into the fully relaxed supercell with polaron followed by localization of that polaron at the V site nearest to the defect. The difference in energies of these two systems gives the binding energy.

III. RESULTS

A. Polaron formation and electronic structure

Table I shows the polaron formation energies E_p for electron and hole polarons in V_xO_y . The more negative the E_p , the greater the preference for polaron localization. Unsurprisingly, holes and electrons prefer to localize on the V^{3+} and V^{4+} , respectively, in the mixed-valence V_3O_5 . In particular, the formation of a hole polaron on the V^{4+} site in V_3O_5 is energetically unfavorable, which is likely due to the fact that V^{5+} generally prefers tetrahedral coordination as it has no $3d$ electrons [49]. Otherwise, polaron localization with lattice distortion is energetically favored over charge delocalization without lattice distortion in all instances. The polaron formation energies in V_3O_5 are of a similar magnitude as the corresponding hole and electron polaron formation energies in V_2O_3 and VO_2 , respectively.

Site	E_p (eV)	
	h^+	e^-
V^{4+} in V_3O_5	+0.05	-0.43
V^{3+} in V_3O_5	-0.21	-0.18
V^{3+} in V_2O_3	-0.31	-
V^{4+} in VO_2	-	-0.52

TABLE I: Formation energies (E_p) for electron and hole polarons at different V sites in V_xO_y .

The polaron localization can be visualized both in terms of the charge density (Figure 2) and the changes in bond lengths around the polaronic site (Figure 3). A decrease in the average bond length of $\sim 3\%$ is observed for hole polaron sites relative to the non-polaronic sites. A similar increase in average bond length is observed for electron polaron sites. These observations are consistent with the fact that higher oxidation states of V would tend to pull the neighboring O closer than lower oxidation states as addition of a hole polaron changes the oxidation state from V^{3+} to V^{4+} (Figure 3) resulting in stronger electrostatic interaction between V and neighbouring O thus causing O atoms to be pulled more closer to V and shorter bond length, by $\sim 3\%$ in this case.

Figure 4 plots the densities of states (DOSs) for all three V-O systems with polarons. In all cases, an additional peak is observed in the forbidden zone due to the trapping of charge. The orbital-projected DOSs show that these additional peaks, along with valence band maxima (VBMs) and conduction band minima (CBMs), have significant contributions from both V-3d and O-2p orbitals indicating a strong hybridization between V and O.

B. Polaron migration barriers

Figure 5 shows the polaron migration pathways in V_xO_y studied in this work. The pathways were determined based on the shortest hops between nearest symmetrically-identical V_3^+/V_4^+ sites using the pymatgen-analysis-diffusion package.

Figure 6 shows the calculated barriers for the various hops in V_xO_y using the linear

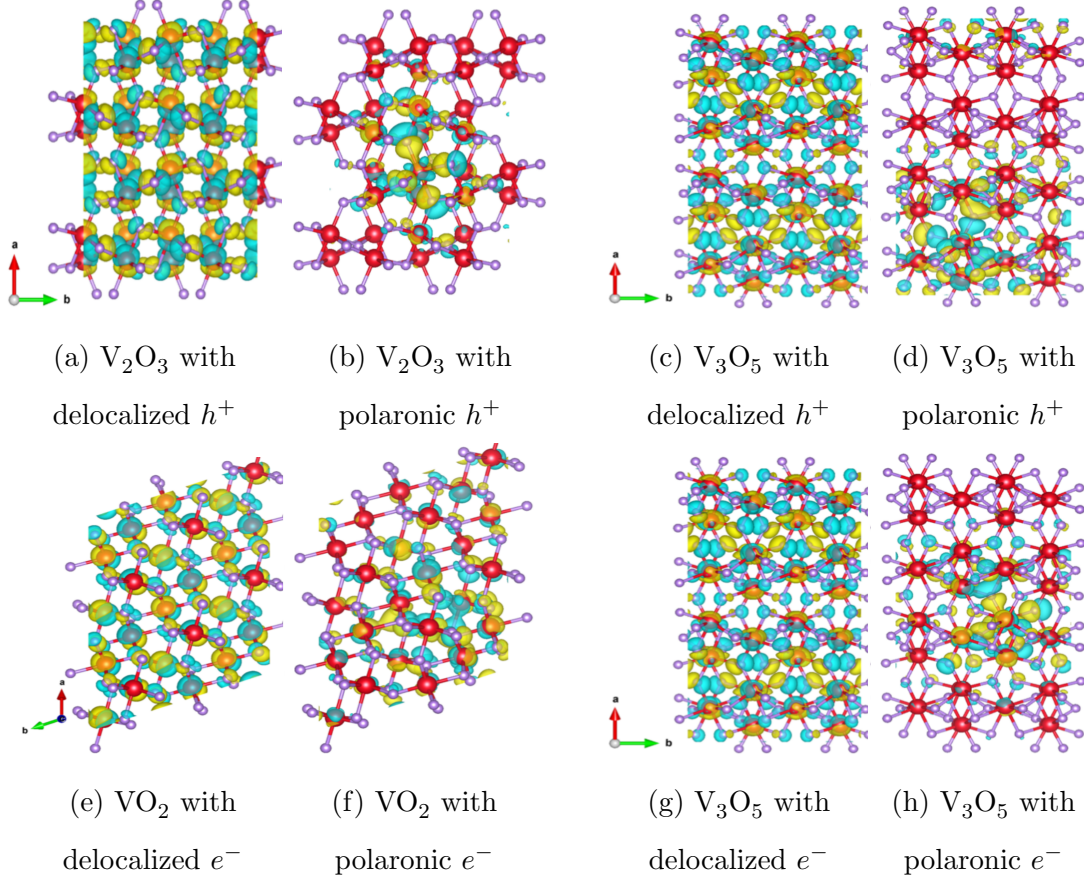


FIG. 2: Charge density isosurfaces for V-O systems with delocalized and polaronic holes (h^+) and electrons (e^-). The cyan and yellow regions represent positive and negative isosurfaces, respectively, with an isovalue magnitude of $0.01360 e^-/\text{\AA}^{-3}$.

interpolated pathways as well as the CI-NEB method. The plots of the energies along the migration coordinates are shown in Figure S1 in the Supplemental Material[50]. It should be noted that the barriers calculated using the CI-NEB method are expected to be lower than the ones from the linearly interpolated images. Interestingly, while the CI-NEB hole polaron migration barriers in V_3O_5 are relatively similar to those in V_2O_3 , the electron polaron migration barriers are much lower than those in VO_2 .

As shown in Figure 5, the hop distances for both hole and electron polarons are relatively similar in all cases. Instead the difference in polaron migration barriers can be explained by the nature of the travelling lattice distortion (Table S1 in the Supplemental Material[50]). In Figure 6, the amount of travelling distortion, defined as the maximum of the average absolute change in V-O bond distance along the CI-NEB pathway, is plotted as well. It can

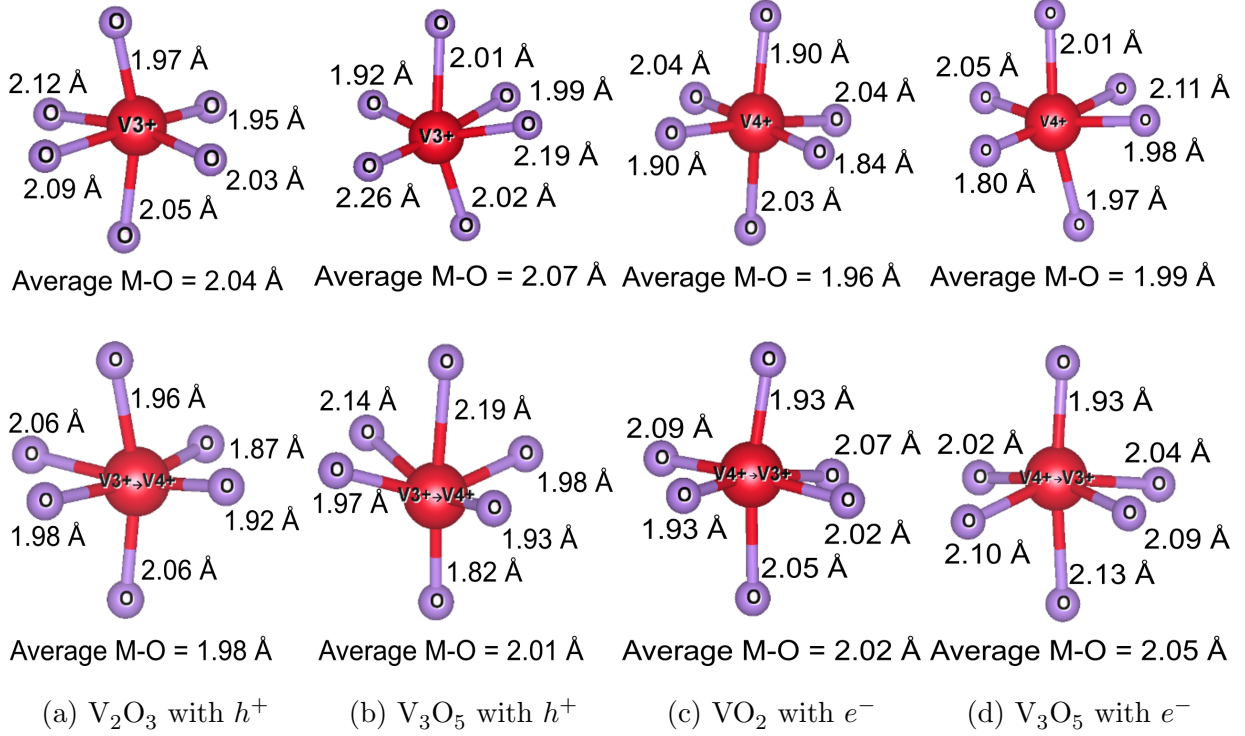


FIG. 3: V-O bond lengths of non-polaronic (top) and polaronic sites (bottom) in V_xO_y systems with hole and electron polarons.

be observed that there is a direct relationship between the amount of the travelling distortion and the CI-NEB migration barrier. In essence, the lower hole and electron polaron migration barriers are the result of a shallower potential energy surface for migration due to smaller bond distortions required to move the polaronic lattice distortion from one site to another.

Using equation 2, we can estimate the polaronic electrical conductivity of the V_3O_5 . For a $2 \times 2 \times 2$ supercell of V_3O_5 with a single polaron, the value of n is $3.57 \times 10^{20} \text{ cm}^{-3}$. With migration barrier of 59 meV for hole polaron and 77 meV for electron polaron along $\{110\}$ direction, the conductivity is calculated to be $\sim 60 \text{ S cm}^{-1}$ at 300 K. The experimentally-measured conductivity value[22] for the low temperature monoclinic V_3O_5 is $\sim 4 \text{ S cm}^{-1}$ at 300 K and $\sim 100 \text{ S cm}^{-1}$ above the MIT temperature of 428K. Hence, hole and electron injection with the formation of polarons can potentially induce a MIT without high temperatures, in agreement with previous experimental studies [21].

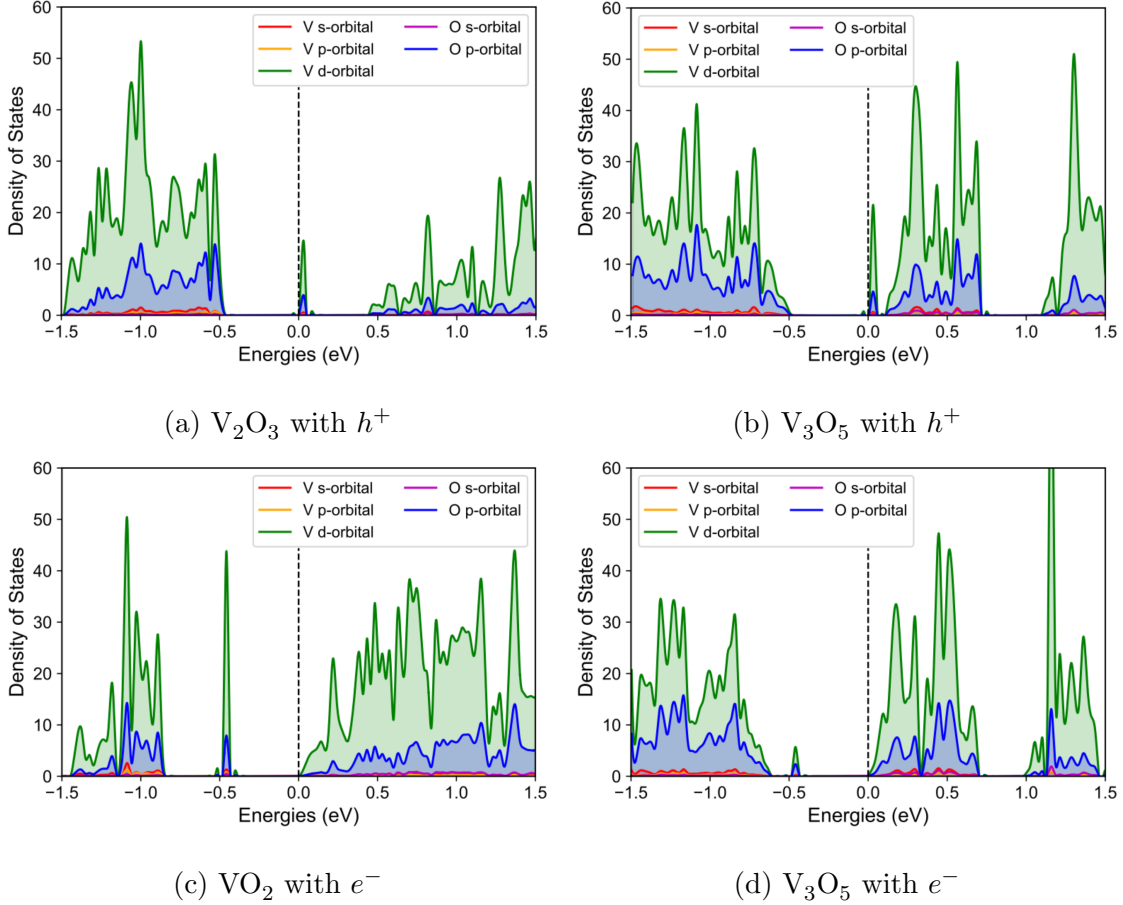


FIG. 4: V-4s (red), V-3p (yellow), V-3d (green), O-2s (magenta), and O-2p (blue) orbital DOS for V_xO_y system with hole and electron polarons. An appearance of additional peak in the forbidden zone is observed for all 4 cases indicating decrease of the gap between occupied and unoccupied levels.

C. Binding energies with point defects

Point defects are often present in V_xO_y [22, 47]. For instance, previous experimental and theoretical results has shown that vanadium vacancies (v_V) tend to form in V_2O_3 under most conditions[6, 51]. Similarly, for VO_2 and V_3O_5 , oxygen vacancies are observed under most conditions[15, 21]. Table II shows the calculated binding energies for different polarons in V_xO_y systems with neutral point defects. While the binding energies are in general much higher than the free polaron migration barriers, the polaron binding energies are much lower in V_3O_5 compared to the corresponding polaron binding energies in VO_2 and V_2O_3 . In particular, the lowest binding energy is between v_O and e^- in V_3O_5 , which is consistent with

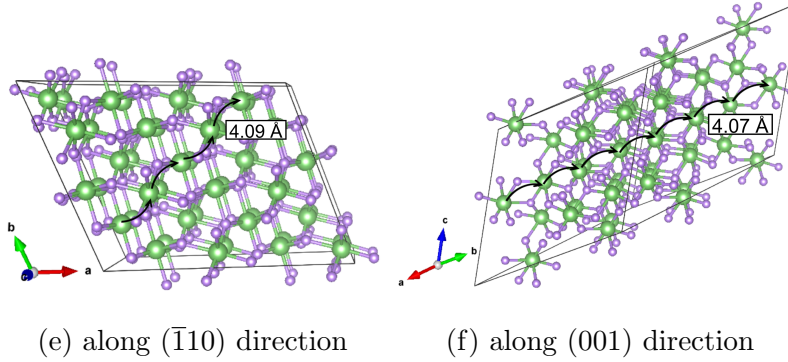
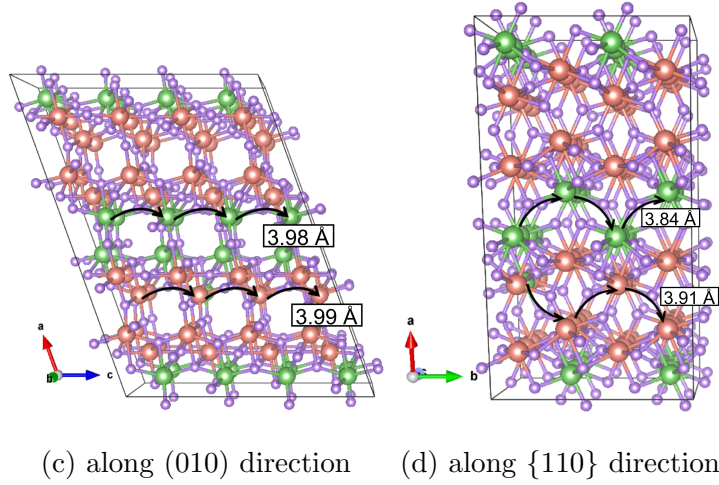
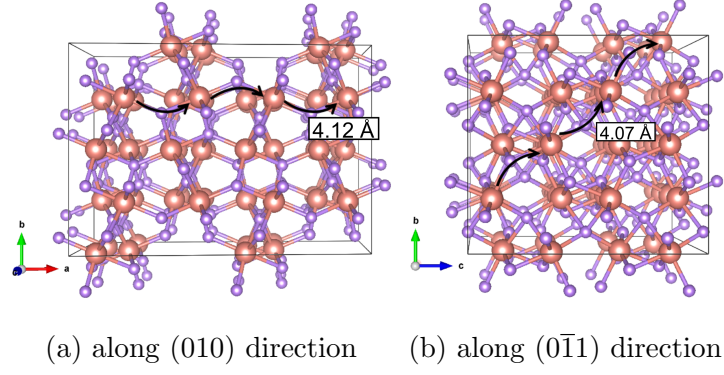


FIG. 5: Polaron hopping paths (shown by black arrows) in V_2O_3 , V_3O_5 and VO_2 explored in this work. The hop distance are indicated in white boxes. The hole polarons hop via V^{3+} ions shown in coral whereas the electron polarons hop through V^{4+} shown in green.

The O atoms are shown in lavender.

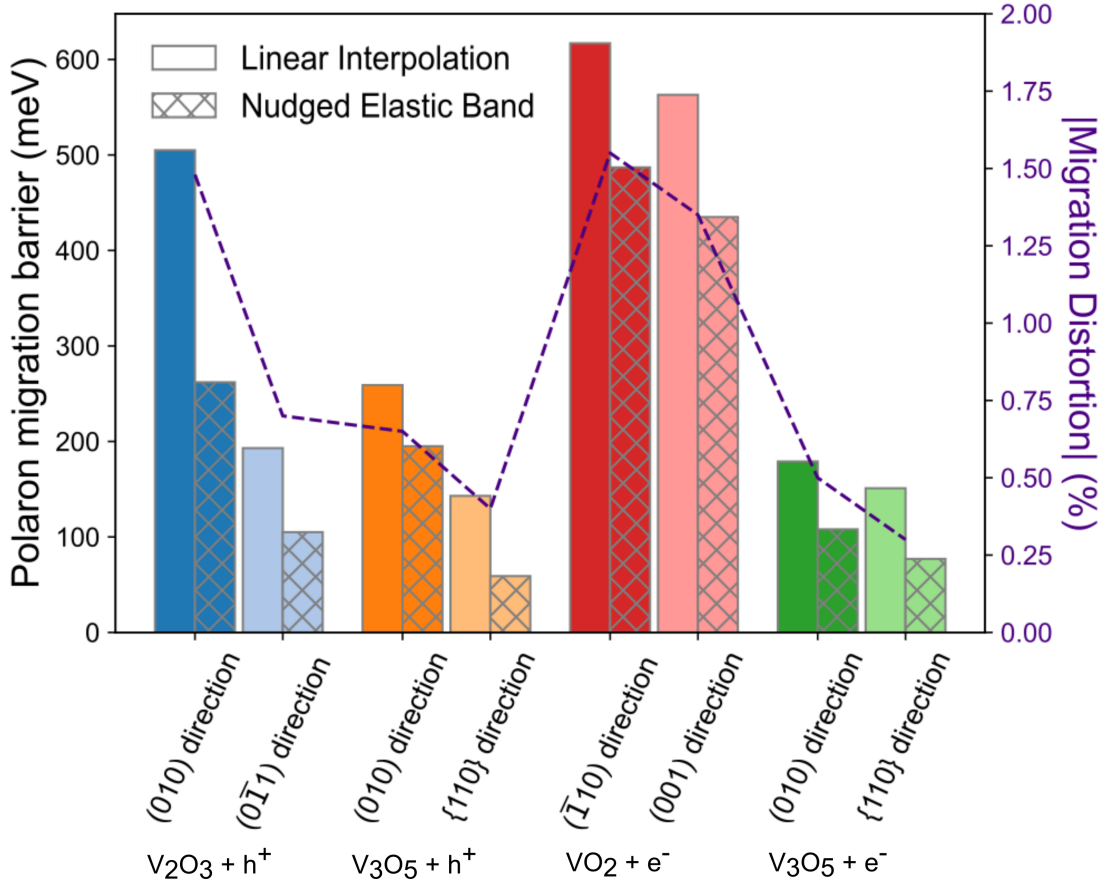


FIG. 6: Calculated free polaron migration barrier from linear interpolation (solid bars) and CI-NEB (checked bars) for V_2O_3 (blue) and V_3O_5 (orange) with hole polaron, and V_3O_5 (green) and VO_2 (red) with electron polaron along their most probable polaron hopping pathways. Visual representation of these pathways can be seen in Figure 5. The purple dashed line indicates the maximum change in average bond length along the migration pathway for each polaron.

recent work showing an optically induced resistive switching based on a CdS/V_3O_5 [21].

IV. CONCLUSION

In conclusion, we have studied polaron-induced MIT in V_2O_3 , V_3O_5 and VO_2 . We find that polaron formation is favored over charge delocalization in all three systems. The lowest barrier for free electron and hole polaron migration were observed in the low-temperature

System	Binding Energy (eV)
$V_2O_3 + v_V + h^+$	0.764
$V_3O_5 + v_O + h^+$	0.477
$V_3O_5 + v_O + e^-$	0.384
$VO_2 + v_O + e^-$	0.948

TABLE II: Comparison of binding energy in case of polaron and neutral point defect containing V-O systems. Here, v_V stands for vanadium vacancy and v_O for oxygen vacancy.

V_3O_5 phase. The resulting polaronic conductivity of V_3O_5 is one order of magnitude higher than the non-polaronic conductivity at room temperature, resulting in a MIT without high temperatures. Polarons in V_3O_5 are also found to bind less strongly to vacancy defects compared to V_2O_3 and VO_2 . These results suggest polaron formation and migration to be the main mechanism behind MIT triggered by the injection of charge carriers.

V. ACKNOWLEDGEMENT

This work was supported by the Quantum Materials for Energy Efficient Neuromorphic Computing (Q-MEEN-C), an Energy Frontier Research Center funded by the U.S. Department of Energy, Office of Science, Basic Energy Sciences under Award # DE-SC0019273. The authors also acknowledge computational resources from the National Energy Research Scientific Computing Center (NERSC), a U.S. Department of Energy Office of Science User Facility located at Lawrence Berkeley National Laboratory, operated under Contract No. DE-AC02-05CH11231.

-
- [1] U. Schwingenschloegl and V. Eyert, *Annalen der Physik* **516**, 532 (2004), arXiv:cond-mat/0403689.
 - [2] H. A. Wriedt, *Bulletin of Alloy Phase Diagrams* **10**, 271 (1989).
 - [3] M.-H. Lee, Y. Kalcheim, J. del Valle, and I. K. Schuller, *ACS Applied Materials & Interfaces* **13**, 887 (2021).

- [4] N. Szymanski, Z. Liu, T. Alderson, N. Podraza, P. Sarin, and S. Khare, *Computational Materials Science* **146**, 310 (2018).
- [5] Y. Zhu, Y. Zhu, H. Mao, Y. He, S. Jiang, L. Zhu, C. Chen, C. Wan, and Q. Wan, *Journal of Physics D: Applied Physics* **55**, 053002 (2021).
- [6] R. Tran, X.-G. Li, S. P. Ong, Y. Kalcheim, and I. K. Schuller, *Physical Review B* **103**, 075134 (2021).
- [7] Y. Wang, K.-M. Kang, M. Kim, H.-S. Lee, R. Waser, D. Wouters, R. Dittmann, J. J. Yang, and H.-H. Park, *Materials Today* **28**, 63 (2019).
- [8] A. Hoffmann, S. Ramanathan, J. Grollier, A. D. Kent, M. J. Rozenberg, I. K. Schuller, O. G. Shpyrko, R. C. Dynes, Y. Fainman, A. Frano, E. E. Fullerton, G. Galli, V. Lomakin, S. P. Ong, A. K. Petford-Long, J. A. Schuller, M. D. Stiles, Y. Takamura, and Y. Zhu, *APL Materials* **10**, 070904 (2022).
- [9] I. K. Schuller, A. Frano, R. C. Dynes, A. Hoffmann, B. Noheda, C. Schuman, A. Sebastian, and J. Shen, *Applied Physics Letters* **120**, 140401 (2022).
- [10] P. Salev, J. del Valle, Y. Kalcheim, and I. K. Schuller, *Proceedings of the National Academy of Sciences* **116**, 8798 (2019).
- [11] G. W. Burr, R. M. Shelby, A. Sebastian, S. Kim, S. Kim, S. Sidler, K. Virwani, M. Ishii, P. Narayanan, A. Fumarola, L. L. Sanches, I. Boybat, M. Le Gallo, K. Moon, J. Woo, H. Hwang, and Y. Leblebici, *Advances in Physics: X* **2**, 89 (2017).
- [12] A. Krishnaprasad, N. Choudhary, S. Das, D. Dev, H. Kalita, H.-S. Chung, O. Aina, Y. Jung, and T. Roy, *Applied Physics Letters* **115**, 103104 (2019).
- [13] A. Jain, S. P. Ong, G. Hautier, W. Chen, W. D. Richards, S. Dacek, S. Cholia, D. Gunter, D. Skinner, G. Ceder, and K. A. Persson, *APL Materials* **1**, 011002 (2013).
- [14] S. Cheng, M.-H. Lee, R. Tran, Y. Shi, X. Li, H. Navarro, C. Adda, Q. Meng, L.-Q. Chen, R. C. Dynes, S. P. Ong, I. K. Schuller, and Y. Zhu, *Proceedings of the National Academy of Sciences* **118**, e2105895118 (2021).
- [15] J. Jeong, J. Jeong, Y. Jung, Y. Jung, Z. Qu, B. Cui, A. Khanda, A. Sharma, S. S. P. Parkin, J. K. S. Poon, and J. K. S. Poon, in *Conference on Lasers and Electro-Optics (2020), Paper STh3R.2* (Optica Publishing Group, 2020) p. STh3R.2.
- [16] W. Yi, K. K. Tsang, S. K. Lam, X. Bai, J. A. Crowell, and E. A. Flores, *Nature Communications* **9**, 4661 (2018).

- [17] E. Corti, B. Gotsmann, K. Moselund, A. M. Ionescu, J. Robertson, and S. Karg, *Solid-State Electronics Special Issue of Solid-State Electronics, Dedicated to EUROSOI-ULIS 2019*, **168**, 107729 (2020).
- [18] N. Shukla, A. Parihar, E. Freeman, H. Paik, G. Stone, V. Narayanan, H. Wen, Z. Cai, V. Gopalan, R. Engel-Herbert, D. G. Schlom, A. Raychowdhury, and S. Datta, *Scientific Reports* **4**, 4964 (2014).
- [19] J. del Valle, P. Salev, F. Tesler, N. M. Vargas, Y. Kalcheim, P. Wang, J. Trastoy, M.-H. Lee, G. Kassabian, J. G. Ramírez, M. J. Rozenberg, and I. K. Schuller, *Nature* **569**, 388 (2019).
- [20] T. Hennen, D. Bedau, J. A. J. Rupp, C. Funck, S. Menzel, M. Grobis, R. Waser, and D. J. Wouters, in *2019 IEEE 11th International Memory Workshop (IMW)* (2019) pp. 1–4.
- [21] C. Adda, H. Navarro, J. Kaur, M.-H. Lee, C. Chen, M. Rozenberg, S. P. Ong, and I. K. Schuller, *Applied Physics Letters* **121**, 041901 (2022).
- [22] A. Rúa, R. D. Díaz, N. Kumar, S. Lysenko, and F. E. Fernández, *Journal of Applied Physics* **121**, 235302 (2017).
- [23] F. A. Chudnovskii, E. I. Terukov, and D. I. Khomskii, *Solid State Communications* **25**, 573 (1978).
- [24] B. Fisher, L. Patlagan, K. B. Chashka, C. Makarov, and G. M. Reisner, *Applied Physics Letters* **109**, 103501 (2016).
- [25] A. Parija, J. V. Handy, J. L. Andrews, J. Wu, L. Wangoh, S. Singh, C. Jozwiak, A. Bostwick, E. Rotenberg, W. Yang, S. C. Fakra, M. Al-Hashimi, G. Sambandamurthy, L. F. J. Piper, R. S. Williams, D. Prendergast, and S. Banerjee, *Matter* **2**, 1166 (2020).
- [26] P. Quémerais and S. Fratini, *International Journal of Modern Physics B* (2012), 10.1142/S0217979298002210.
- [27] L. T. A. Thu, N. N. Dinh, N. V. Tuyen, and B. T. Cong, *Bulletin of Materials Science* **43**, 139 (2020).
- [28] D. V. Averyanov, O. E. Parfenov, A. M. Tokmachev, I. A. Karateev, O. A. Kondratev, A. N. Taldenkov, M. S. Platunov, F. Wilhelm, A. Rogalev, and V. G. Storchak, *Nanotechnology* **29**, 195706 (2018).
- [29] M. H. Khan, S. Pal, and E. Bose, *Physica Scripta* **90**, 035803 (2015).
- [30] N. Kumar, A. Rúa, J. Lu, F. Fernández, and S. Lysenko, *Physical Review Letters* **119**, 057602 (2017).

- [31] W. Kohn and L. J. Sham, *Physical Review* **140**, A1133 (1965).
- [32] G. Kresse and J. Furthmüller, *Physical Review B* **54**, 11169 (1996).
- [33] G. Kresse and J. Hafner, *Physical Review B* **47**, 558 (1993).
- [34] G. Kresse and J. Furthmüller, *Computational Materials Science* **6**, 15 (1996).
- [35] P. E. Blöchl, *Physical Review B* **50**, 17953 (1994).
- [36] J. P. Perdew, K. Burke, and M. Ernzerhof, *Physical Review Letters* **77**, 3865 (1996).
- [37] J. P. Perdew, J. A. Chevary, S. H. Vosko, K. A. Jackson, M. R. Pederson, D. J. Singh, and C. Fiolhais, *Physical Review B* **46**, 6671 (1992).
- [38] P. E. Blöchl, O. Jepsen, and O. K. Andersen, *Physical Review B* **49**, 16223 (1994).
- [39] S. P. Ong, W. D. Richards, A. Jain, G. Hautier, M. Kocher, S. Cholia, D. Gunter, V. L. Chevrier, K. A. Persson, and G. Ceder, *Computational Materials Science* **68**, 314 (2013).
- [40] B. Himmetoglu, A. Floris, S. de Gironcoli, and M. Cococcioni, *International Journal of Quantum Chemistry* **114**, 14 (2014).
- [41] S. P. Ong, V. L. Chevrier, and G. Ceder, *Physical Review B* **83**, 075112 (2011).
- [42] S. P. Ong, Y. Mo, and G. Ceder, *Physical Review B* **85**, 081105 (2012).
- [43] W. Tang, E. Sanville, and G. Henkelman, *Journal of Physics: Condensed Matter* **21**, 084204 (2009).
- [44] Y. Natanzon, A. Azulay, and Y. Amouyal, *Israel Journal of Chemistry* **60**, 768 (2020).
- [45] G. Henkelman, B. P. Uberuaga, and H. Jónsson, *The Journal of Chemical Physics* **113**, 9901 (2000).
- [46] A. Moradabadi and P. Kaghazchi, *Physical Review Applied* **7**, 064008 (2017).
- [47] D. Wickramaratne, N. Bernstein, and I. I. Mazin, *Physical Review B* **99**, 214103 (2019).
- [48] C. Franchini, M. Reticioli, M. Setvin, and U. Diebold, *Nature Reviews Materials* **6**, 560 (2021).
- [49] J. B. Goodenough, *Annual Review of Materials Science* **1**, 101 (1971).
- [50] See Supplemental Material at [URL] for further details of polaron migration with respect to its energetics, distortion and its visual representation in V_xO_y systems.
- [51] V. Simic-Milosevic, N. Nilius, H.-P. Rust, and H.-J. Freund, *Physical Review B* **77**, 125112 (2008).